ANALYSIS OF CAUSE AND MECHANISM FOR INJECTION-INDUCED SEISMICITY AT THE GEYSERS GEOTHERMAL FIELD, CALIFORNIA

Jonny Rutqvist and Curtis Oldenburg
Lawrence Berkeley National Laboratory, Berkeley, CA 94720

Key words - Induced seismicity, Geysers, Injection, geomechanical modeling

ABSTRACT

We analyzed relative contributions to the cause and mechanism of injection-induced seismicity at The Geysers geothermal field, California, using coupled thermal-hydrological-mechanical modeling. Our analysis shows that the most important cause for injection-induced seismicity is injection-induced cooling and associated thermal-elastic shrinkage that changes the stress state in such a way that mechanical failure and seismicity can be induced. Specifically, the cooling shrinkage results in unloading and associated loss of shear strength in critically shear-stressed fractures, which are then reactivated. Thus, our analysis shows that cooling-induced shear slip along fractures is the dominant mechanism of injection-induced seismicity at The Geysers.

INTRODUCTION

At the Geothermal Resources Council (GRC) Annual Meeting in 2006, we presented a coupled thermal-hydrological-mechanical (THM) analysis of induced seismicity at The Geysers (Rutqvist et al., 2006). The potential for induced seismicity was determined by calculating changes in stress (in time and space) and investigating if those changes could induce a rock mechanical failure and associated seismicity. An important aspect of the analysis was the concept of a rock mass that is critically stressed for shear failure. The concept of a critically stressed rock mass at The Geysers arose from studies in the early 1980's by Lockner et al. (1982) and Oppenheimer (1986). For example Lockner et al. (1982) suggested that shear stress in the region is near the rock-mass frictional strength, and therefore very small perturbations of the stress field could trigger seismicity. The results presented in our 2006 GRC paper, focusing on seismicity induced by steam production, were in agreement with earlier analyses, including those by Oppenhiemer in the 1980's and more recent studies by Mossop (2001). For example, our analysis showed that shallow production-induced seismicity are caused by poro-elastic stress transfer during pressure depletion of the underlying reservoir, whereas the deep production-induced seismicity could be explained by thermo-elastic stresses resulting from evaporative cooling.

In this paper we present new results focusing on injection-induced seismicity. The analysis is conducted using a similar model setup and simulation approach as in our previous study, but we introduce cold water injection in addition to the steam production.

MODEL SETUP AND APPROACH

The coupled THM analysis was conducted with TOUGH-FLAC (Rutqvist et al., 2002), a simulator based on linking the geothermal reservoir simulator TOUGH2 with the geomechanical code FLAC^{3D}. We conducted the simulations on a simplified two-dimensional model representing one-half of a NE-SW cross-section of the NW-SE trending Geysers geothermal

field (Figure 1). Data from published papers (e.g. Williamson, 1992) were used to constrain a conceptual model of the field, including a low-permeability cap and a very-low-permeability lateral boundary that define limits of a reservoir approximately 10 km wide by 3 km deep (Figure 1). The equivalent fractured rock permeability in the reservoir is $1 \cdot 10^{-14}$ m^2 (10 millidarcy) with a 2% porosity. The grid, taking advantage of symmetry, models a 5 km wide section in the northeastern part of The Geysers. The initial (pre-production) conditions were established through a steady state multi-phase flow simulation. The initial reservoir temperature of about 240°C down to depth of 3.5 km and then gradually increasing to 350°C towards the bottom boundary at a depth of 5.5 km. The initial steam pressure within the reservoir is a bout 4 MPa, whereas the pressure outside the sealed reservoir is equal to hydrostatic water pressure.

Because the state of maximum and minimum compressive principal effective stresses, σ'_1 and σ'_3 respectively, is initially considered to be on or near a state of failure, we analyze the likelihood of induced seismicity by investigating if active production/injection moves the state of stress away from or toward a condition of failure. Applying a Coulomb failure criterion and a conservative choice of friction angle of 30°, the onset of shear failure could occur if the maximum principal compressive effective stress exceeds three times the minimum principal effective stress (i.e., if $\sigma'_1 \geq 3 \times \sigma'_3$, failure is likely). This implies that the state of stress would move towards failure if the change in maximum principal compressive effective stress exceeds three times the change in minimum principal effective stress (i.e., if $\Delta\sigma'_1 \geq 3 \times \Delta\sigma'_3$, failure is likely). Conversely, if $\Delta\sigma'_1 < 3 \times \Delta\sigma'_3$, failure is unlikely. Moreover, we investigate the potential for failure by comparing changes in maximum principal stress to the critical changes in maximum principal stress for failure, i.e., $\Delta\sigma'_{1m} = \Delta\sigma'_1 - \Delta\sigma'_{1c} = \Delta\sigma'_1 - 3 \times \Delta\sigma'_3$.

The potential causes and mechanisms of injection-induced seismicity were studied at two temporal scales:

      1) Analysis of 44 years of production/injection from 1960 to 2004;

      2) Analysis of seasonal injection cycles during 2005.

Steam was produced at the left-hand side (mirror plane) boundary of the two-dimensional Cartesian model between 1,600 to 3,000 m depth, and water was injected at a distance of 217 m from the left boundary of the model, also between 1,600 to 3,000 m depth. The steam production and injection rates were derived from field wide data at The Geysers from 1960 through 2005 shown in Figure 2 (Stark et al. 2005, and Stark personal communication). For our two-dimensional (1 meter thick) simulation model, the field-wide production/injection rates were reduced to a factor approximately $5 \cdot 10^{-5}$ of the values shown in Figure 2. This fraction arises from geometric considerations such as the difference in width of the model and actual system. Specifically, the Geysers field is 13 km long while our two-dimensional Geysers model is 1 m wide. This difference corresponds to a factor of $1.3 \cdot 10^4$ reduction in production and injection rates relative to the actual Geysers field. The remaining reduction by a factor of approximately 1.5 can be explained by fact that we are modeling a two-dimensional slice as opposed to a radial system, which would allow for radial in/out flow. For the production well, the rate was further halved to correspond to a mirror plane in the conceptual model of the system. For the analysis of 44 years production/injection yearly average values were used whereas monthly values were

used for the analysis of seasonal injection cycles. We emphasize that the two-dimensional cross-section model and the production and injection rates we are using are not meant to be a precise model of the Geysers system, but rather an analog model capable of representing fundamental processes of THM coupling.

ANALYSIS OF 44 YEARS OF PRODUCTION/INJECTION

The simulation of 44 years of steam-production and injection resulted in a reservoir-wide pressure and temperature decline of a few MPa and a few degrees, respectively, as well as subsidence of about 0.5 to 1 meter. These numbers are in general agreement with field observations at the Geysers (Mossop and Segall,1997). In the simulations, a rock-mass bulk modulus of 3 GPa was adopted, which approximately corresponds to values back-calculated by Mossop and Segall (1997), using analytical strain analyses. The thermal expansion coefficient was set to 3×10^{-5} °C^{-1}, which corresponds to values determined on core samples of the reservoir rock at high (250°C) temperature (Mossop and Segall, 1997).

Figure 3 shows calculated liquid saturation and changes in fluid pressure and temperature after 44 years of production/injection. Figure 3a shows that the injection caused formation of a wet zone that extends all the way to the production well as well as downwards, about 1,000 m below the injection well. Figure 3c indicates a local cooling effect wherever the water flows, especially where the liquid reaches the production well. The injection has a significant effect on the fluid pressure at depths towards the bottom of the model, where pressure depletion is prevented (Figure 3b).

Figures 4a and b depict changes in vertical and horizontal effective stresses, respectively. The stress change in the rock mass is caused by both production-induced depletion and injection-induced cooling. The depletion and cooling causes a general shrinkage of the reservoir, which in turn give rise to increased horizontal stresses near the ground surface (Figure 4a). The main effect of water injection is a reduction of vertical effective stress within the zone of cooling. The cooling shrinkage near the wells is stronger in the vertical direction because the zone of cooling is elongated vertically.

Figure 4c shows the calculated distribution of failure potential, which is represented by the parameter $\Delta\sigma'_{1m} = \Delta\sigma'_1 - \Delta\sigma'_{1c}$ described above. In Figure 4c, red and yellow contours are the zones that are most prone to failure, whereas blue contours are zones that are least prone to failure. The figure indicates that failure (and induced seismicity) caused by production/injection would occur both near the ground surface and close to the wells, and at depth below the wells (Figure 4c).

ANALYSIS OF SEASONAL INJECTION CYCLES

We analyzed the effects of seasonal injection cycles corresponding to 2005 production/injection rates. Our initial conditions are those achieved at the end of the 44-year simulation period, from 1960 to 2004. Thus, in this case we study mechanical changes that occur during 12 months with respect to the mechanical state at the end of December 2004.

Figure 5 presents the basic thermal-hydrological responses, i.e., liquid saturation, and changes in fluid pressure and temperature, after 6 months. The seasonal injection, which peaks at about 1 to 2 months, produces a pulse of liquid flow that travels along the existing wet zone, towards the production well and downwards about 1,000 m below the wells. For example, comparing Figure 5a with Figure 4a we can see some increased liquid saturation within the wet zone. This pulse causes a pressure increase and cooling near the bottom of the wet zone when the liquid water hits dryer and hotter rocks (Figure 5b and c).

Figure 6 shows the calculated distributions of stress changes and failure. Zones of high potential for failure occurs along the injection borehole an around the zone of cooling and elevated fluid pressure at the bottom of the wet zone, i.e., about 1,000 m below the injection well. Along the borehole, the zone of failure (Figure 6c) correlates with the zone of cooling (Figure 5c) and reduced vertical effective stress (Figure 6b). The failure zone located 1,000 m below the injection well (Figure 6c) correlates with the zone of cooling (Figure 5c) and the zone of reduced effective stresses (Figure 6a and b). The mechanism of failure (and induced seismicity) is shear reactivation of fractures caused by a reduction in frictional strength as effective stresses are reduced, which in turn is caused by cooling shrinkage and to a smaller extent by elevated fluid pressure at depths.

Figure 7 compares the time evolution of injection rate and potential for failure (($\Delta\sigma'_m = \Delta\sigma'_1 - \Delta\sigma'_{1c}$). Overall, the simulation results indicate that near the injection well there is a time lag of a few months (Figure 7a), which is related to the time it takes for the injected cold water to induce local rock cooling. At 5,000 m depth, the longer time lag is related to the time it takes for the fluid pressure to propagate downwards and reduce the effective stresses (Figure 7b).

CONCLUSIONS

We analyzed the cause and mechanism of induced seismicity at The Geysers geothermal field, California, using coupled thermal-hydrological-mechanical numerical modeling. Our results are in qualitative agreement with field observations (e.g., Stark 2003). Specifically, both modeling and field observations show that most of the injection-induced seismicity occurs near injection and production wells, and can spread several kilometers below injection wells. Moreover, the analysis shows a typical time lag between seasonal peak injection rates and peaks in induced seismicity. Based on our analysis, we draw the following specific conclusions regarding relative contributions to the cause and mechanism of induced seismicity at The Geysers:

- Shear slip along existing fractures as a result of reduced minimum principal compressive stress is the most likely mechanism of induced-seismicity at The Geysers.

- Near injection and production wells, thermal-elastic cooling shrinkage is the dominant cause for stress changes leading to injection-induced seismicity.

- At greater depths below production and injection wells, both thermal-elastic cooling shrinkage and increased fluid pressure as a result of injection may contribute to reducing effective stress leading to deep injection-induced seismicity.

- Injection-induced seismicity could also occur in the shallow parts of the system and in the cap rock caused by stress redistribution from injection-induced cooling shrinkage within the underlying reservoir.

Future modeling will include injection into a discrete high permeable vertical fracture, which could explain fast propagation and short time lag between injection and seismicity located far below the injection wells as observed in Stark (2003).

REFERENCES

Lockner D.A., Summer R., Moore D., and Byerlee J.D., 1982. Laboratory measurements of reservoir rock from the Geysers Geothermal Field, California. *Int. J. Rock mech. Min. Sci.* 19, 65-80.

Mossop A.P. 2001. Seismicity, subsidence and strain at The Geysers geothermal field. Ph.D. dissertation, Stanford University.

Mossop A.P., and Segall, P., 1997. Subsidence at The Geysers geothermal field, N. California from a comparison of GPS and leveling surveys. *Geophys. Res. Letter* 24, 1839–1842.

Oppenheimer, D.C., 1986. Extensional tectonics at the Geysers Geothermal Area, California, *J. Geophys. Res.*, 91, 11463–11476.

Rutqvist J., Wu, Y.-S., Tsang, C.-F., and Bodvarsson, G., 2002. A Modeling Approach for Analysis of Coupled Multiphase Fluid Flow, Heat Transfer, and Deformation in Fractured Porous Rock *Int. J. Rock mech. Min. Sci.* 39, 429-442.

Rutqvist J., Majer E., Oldenburg C., Peterson J., and Vasco D. 2006. Integrated modeling and field study of potential mechanisms for induced seismicity at The Geysers Geothermal Field, California. *GRC Transactions*, 30, 629-633.

Stark, M.A. 2003 Seismic evidence for a long-lived enhanced geothermal system (EGS) in the Northern Geysers Reservoir, *GRC Transactions*, 27, 727-731.

Stark, M.A., Box W.T., Beall J.J., Goyal K.P., and Pingol A.S. 2005. The Santa Rosa-Geysers recharge project, Geysers Geothermal Field, California, *GRC Transactions*, 29, 145-150.

Williamson, K.H. 1992. Development of a reservoir model for the Geysers Geothermal Field, Monograph on The Geysers Geothermal Field, Geothermal Resources Council, *Special Report no. 17*, 179-187.
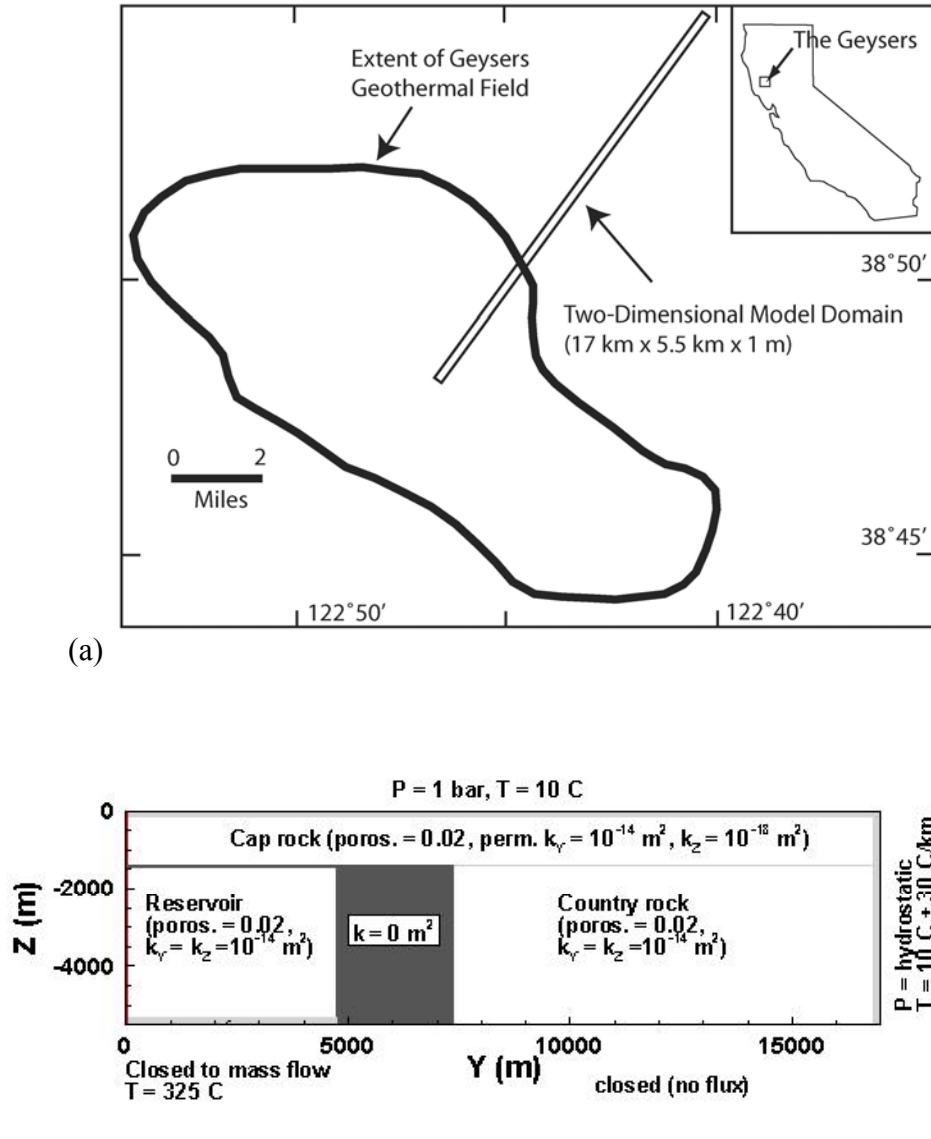
(a)

(b)

Figure 1. Two-dimensional model for coupled THM analysis of induced seismicity at The Geysers. (a) Location map of The Geysers showing approximate boundary of the geothermal reservoir and orientation of the two-dimensional model domain and (b) model geometry with hydraulic properties of different rock units and boundary conditions.
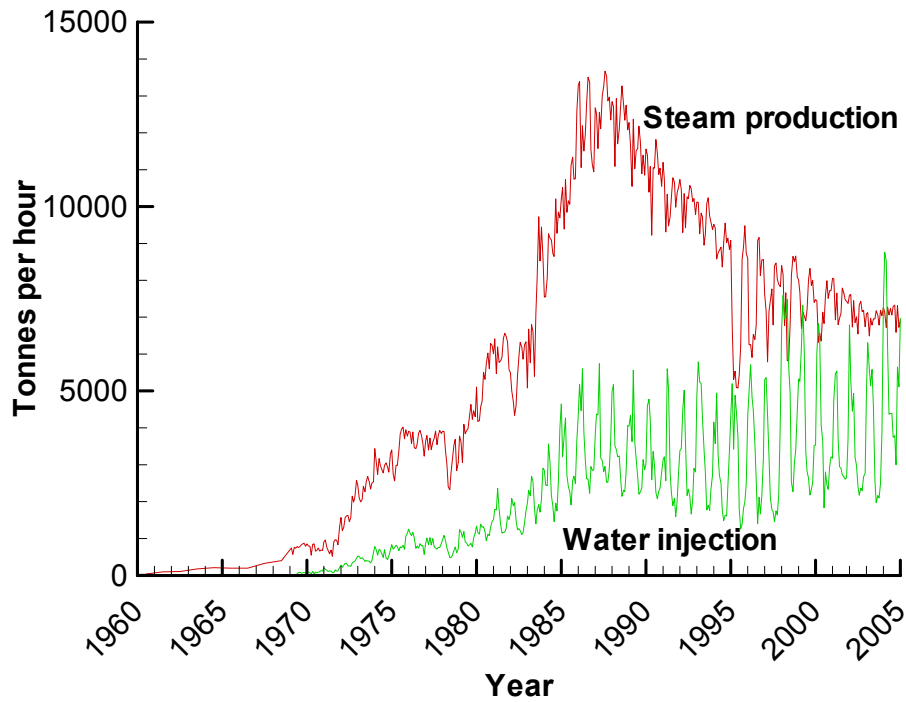
Figure 2. The Geysers reservoir wide steam-production and water-injection rates from 1960 to 2005 used as basis for input to the coupled THM analysis (data also shown in Stark et al. (2005) and were obtained from M. Stark of Calpine by personal communication).

Figure 3. Calculated basic thermal-hydrological responses after 44 years of production/injection. (a) liquid saturation, (b) change in fluid pressure, and (c) change in temperature.
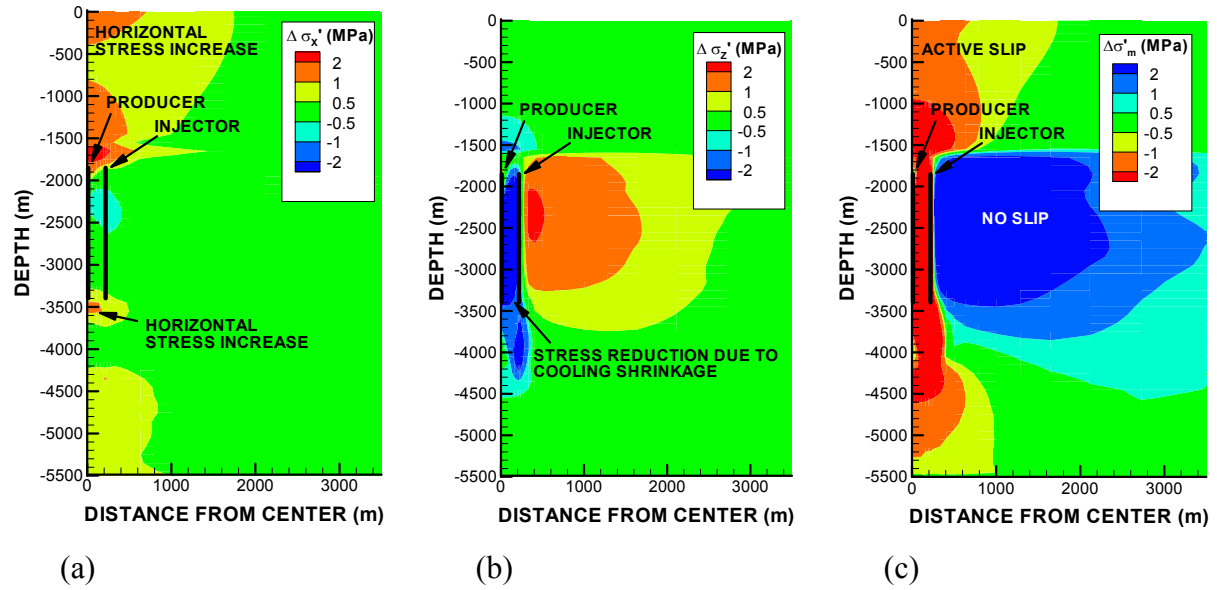
Figure 4. Calculated geomechanical responses after 44 years of production/injection. Changes in (a) horizontal effective stress (b) vertical effective stress and (c) potential for failure, $\Delta\sigma'_{1m} = \Delta\sigma'_1 - \Delta\sigma'_{1c}$.
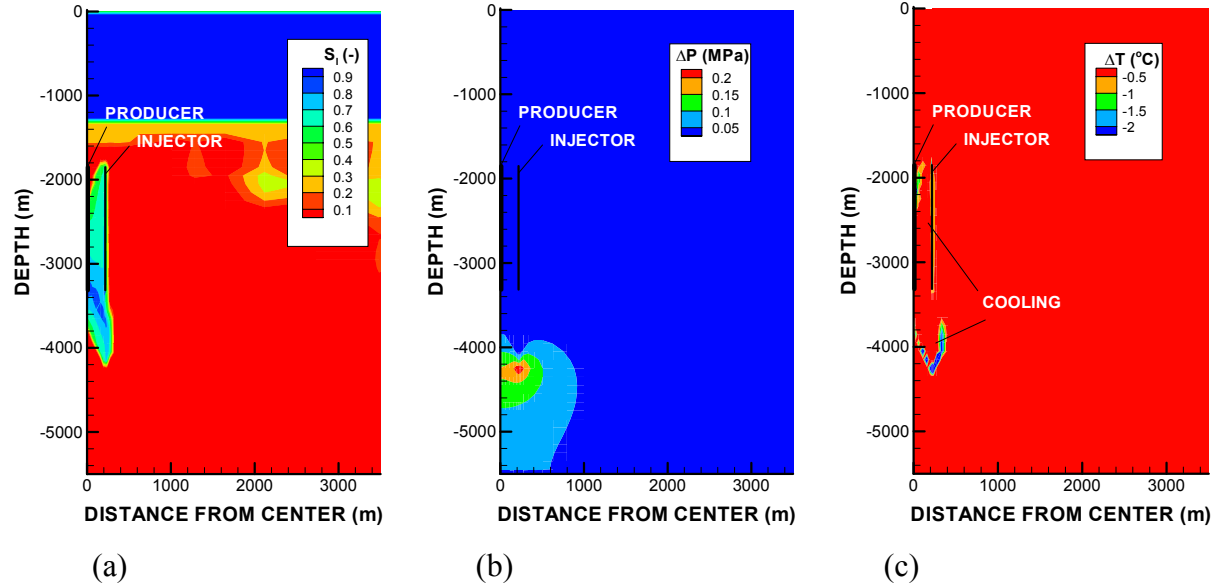

Figure 5. Calculated basic thermal-hydrological responses after 6 months of the 2005 seasonal injection analysis. (a) liquid saturation, (b) changes in fluid pressure, and (c) changes in temperature.
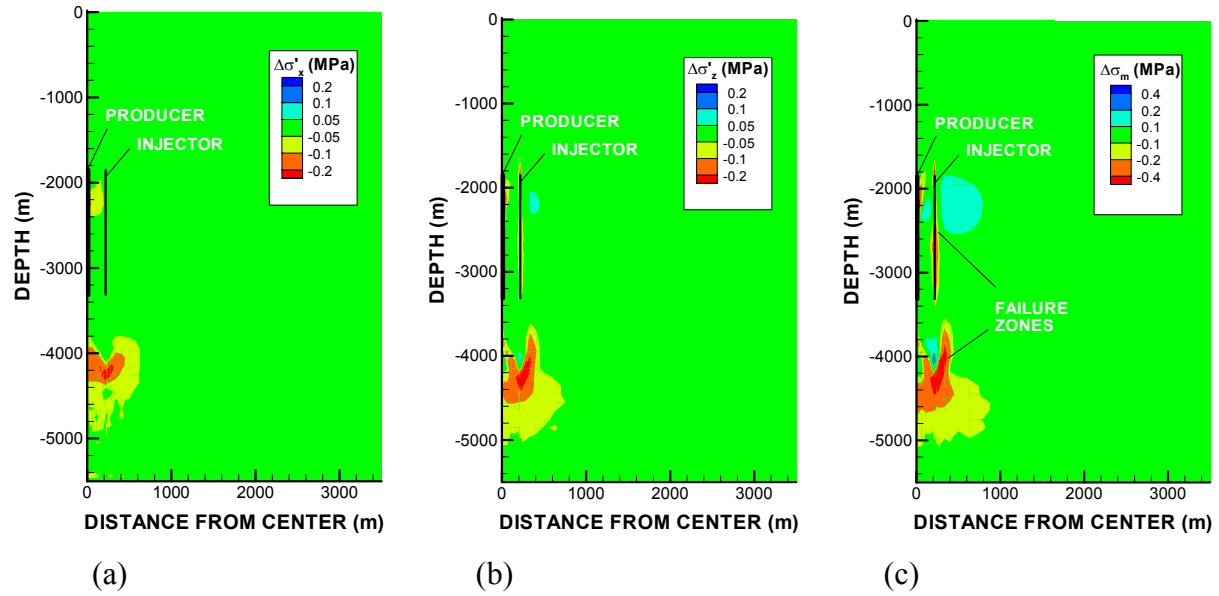
Figure 6. Calculated geomechanical responses after 6 months of the 2005 seasonal injection. Changes in (a) horizontal effective stress (b) vertical effective stress and (c) potential for failure, $\Delta\sigma'_{1m} = \Delta\sigma'_1 - \Delta\sigma'_{1c}$.
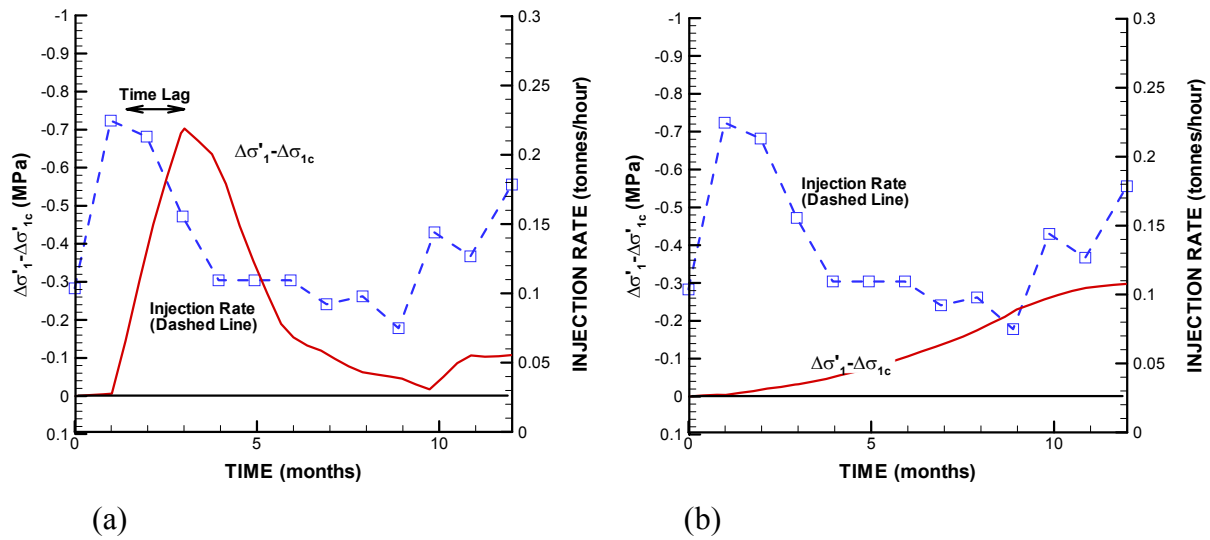

Figure 7. Comparison of injection rate and evolution of failure margin ($\Delta\sigma'_1 - \Delta\sigma'_{1c}$) at (a) the bottom of the injection well ($x = 217.5$ m, $z = -3325$ m), and at (b) about 1700 m below the injection well ($x = 217.5$ m, $z = -5000$ m).